15 Dec 2007

Effect of Sparger Design on Hydrodynamics of a Gas Recirculation Anaerobic Bioreactor

Rajneesh Varma

Muthanna H. Al-Dahhan
Missouri University of Science and Technology, aldahhanm@mst.edu

Recommended Citation

R. Varma and M. H. Al-Dahhan, "Effect of Sparger Design on Hydrodynamics of a Gas Recirculation Anaerobic Bioreactor," *Biotechnology and Bioengineering*, vol. 98, no. 6, pp. 1146 - 1160, Wiley, Dec 2007. The definitive version is available at https://doi.org/10.1002/bit.21500

eppendorf

Boost Your (Stem) Cell Culture

We assist you to scale up your bioprocess –
Eppendorf Bioprocess Solutions for Cell & Gene Therapy Development - Flexibe, Scalable, Industrial

The BioFlo® 320 offers flexibility, better control, and maximum functionality while occupying a fraction of the valuable lab space of similar systems. This means greater efficiency and productivity at a lower operating cost for your lab. BioBLU® Single-Use Bioreactors were developed as true replacements for existing reusable vessels.

- > Sterility Assurance Level (SAL): 10^{-6}
- > Simplified handling reduces cross-contamination
- > Reliable scalability from 250 mL - 40 L through industrial design
- > Proven for animal and human cell lines
- > Increased productivity with reduced turnaround time between runs

www.eppendorf.com/BioBLUc

ARTICLE

BIOTECHNOLOGY and BIOENGINEERING

Effect of Sparger Design on Hydrodynamics of a Gas Recirculation Anaerobic Bioreactor

Rajneesh Varma, Muthanna Al-Dahhan

Bioreactors and Bioprocess Engineering Laboratory (BBEL), Chemical Reaction Engineering Laboratory (CREL), Department of Energy Environmental and Chemical Engineering, Urbauer Hall #208 Campus Box 1198, One Brookings Dr., Washington University, St. Louis, Missouri 63130; telephone: +1-314-935-7187; fax: +1-314-935-4832; e-mail: muthanna@seas.wustl.edu

Received 20 February 2007; revision received 23 April 2007; accepted 8 May 2007

Published online 18 May 2007 in Wiley InterScience (www.interscience.wiley.com). DOI 10.1002/bit.21500

ABSTRACT: The effects of sparger design and gas flow rate on, gas holdup distribution and liquid (slurry) recirculation velocity have been studied in a surrogate anaerobic bioreactor used for treating bovine waste with a conical bottom mixed by gas recirculation. A single orifice sparger (SOS) and a multi-orifice ring sparger (MORS) with the same orifice open area and gas flow rates (hence the same process power input) are compared in this study. The advanced non-invasive techniques of computer automated tomography (CT) and computer automated radioactive particle tracking (CARPT) were employed to determine gas holdup, liquid recirculation velocity, and the poorly mixed zones. Gas flows (Q_g) ranging of 0.017×10^{-3} m^3/s to 0.083×10^{-3} m^3/s were used which correspond to draft tube superficial gas velocities ranging from 1.46×10^{-2} m/s to 7.35×10^{-2} m/s (based on draft tube diameter). Air was used for the gas, as the molecular weights of air and biogas (consisting mainly of CH_4 and CO_2) are in the same range (biogas: 28.32–26.08 kg/kmol and air: 28.58 kg/kmol). When compared to the SOS for a given gas flow rate, the MORS gave better gas holdup distribution in the draft tube, enhanced the liquid (slurry) recirculation, and reduced the fraction of the poorly mixed zones. The improved gas holdup distribution in the draft tube was found to have increased the overall liquid velocity. Hence, for the same process power input the MORS system performed better by enhancing the liquid recirculation and reducing the poorly mixed zones.

Biotechnol. Bioeng. 2007;98: 1146–1160.

KEYWORDS: CARPT; CT; bioreactor; sparger design; power input

Introduction

Animal waste from agricultural sources is a source of largely unexplored renewable energy. It is estimated that about 230 million tons of animal waste (dry weight basis) are generated in the United States annually (Sheffield, 2002). Most of it is discharged untreated, a potential source of pollution. Methane, a gas with higher green house potential than carbon dioxide, is generated from the waste and could be utilized as an energy source and thereby reduce its potential green house effect. Anaerobic bioreactors readily generate methane for energy utilization from such waste. Moreover, the liquid/semisolid byproduct is an excellent soil conditioner.

Over the last couple of decades the anaerobic digestion process has been applied to different kinds of agricultural, animal, and industrial wastes (Gosh, 1997; Speece, 1996). Many configurations have been tested and employed in lab scale and large-scale systems. However, in a Department of Energy sponsored study by Lusk (1998), which covered about a hundred field anaerobic bioreactors, it was reported that 60% of them have failed. Mechanical problems associated with mixing were identified as one of the major reasons.

As in all heterogeneous reaction systems, mixing plays an important role in the performance of anaerobic bioreactors. The process of degradation is facilitated by anaerobic microorganisms that are in nature. Mixing facilitates contact between the microbial flocs and the solid suspended matter, as well as the dissolved matter that constitutes the substrate. Mixing also prevents scum formation, settling of the solids and reduction in poorly mixed zones, thereby enabling smooth operation. Hence, a better understanding of the

Correspondence to: M. Al-Dahhan
Contract grant sponsor: US Department of Energy (DOE)
Contract grant number: DE-FC36-01GO11054

mixing process is required to improve the performance of such bioreactors.

Since the objective of commercially viable anaerobic degradation is to generate net energy while disposing of waste, the amount of process energy that can be invested is limited by the quantity of energy generated from the methane produced. Although the other byproducts such as the solid sludge, has great potential as soil conditioner and fertilizer, its commercial value is limited. Typically, the modes of mixing in anaerobic bioreactors can be broadly classified as impeller-based agitation, liquid jets or slurry recirculation, and gas recirculation. High mixing rates may yield better performance in biogas generation; however when the process energy requirement is weighed against the energy from the biogas generated, a process with high mixing rates becomes economically unviable. Also, very high mixing rates may cause destruction of the microbial population (Stroot et al., 2001; Whitmore et al., 1987), which would lead to the failure of the bioreactor. It is for this reason that impeller-based reactors and circulating liquid jets are not popular.

Gas recirculation bioreactors are a more appealing option as they have no moving parts and their energy requirements are minimal. In these reactors the biogas generated is recirculated with the aid of blowers. It must be noted that the gas in anaerobic processes is used purely to induce mixing and does not consists of any species that participates in reaction or in the cell growth process. In contrast, gas (air) used in aerobic process has a species (oxygen) that participates in the cell growth processes. Therefore, requirements for high gas holdup or a high gas-liquid interfacial area, to facilitate mass transfer of any species from the gas phase to the liquid phase do not exist in the anaerobic bioreactors. This basic reality makes a significant impact on the operating conditions and design of gas mixed bioreactors for anaerobic digestion applications. According to an estimate by Chisti (1998), aerobic reactors that are gas (air) agitated require 3000–2000 W/m^3 to meet the dissolved oxygen and mixing requirements for systems that produce primary metabolites from microorganisms or that treat effluent. For gas mixed anaerobic systems the EPA (US EPA, 1979) recommends a power input range of 5–8 W/m^3.

In this work, the effect of a single orifice sparger (SOS) system, also called an ejector, on mixing and hydrodynamics has been compared with that of a multi-orifice ring sparger (MORS). The gas phase distribution, the liquid velocity profile, and the liquid flow pattern visualization studies have been conducted for the same superficial gas velocities in both the systems. Such comparison will indicate the impact of the degree of uniformity of gas holdup in the draft tube on the formation of the poorly mixed zones in the system. These studies have been done with the synergistic use of single source gamma ray computer tomography (CT) and computer automated radioactive particle tracking (CARPT). CARPT and CT are not hindered by typical opacity of reactor walls and its contents. CARPT enables mapping the flow field of a particular phase (solid or liquid) in a given system. CT employs the penetrable property of gamma-ray photons to image the holdup, or spatial distribution, of a particular phase at a given cross sectional level in any system.

Materials and Methods

Methods

Details of the Surrogate Anaerobic Bioreactor

The experiments were carried out in a 6 in. (15.24×10^{-2} m) diameter bioreactor with a conical bottom and a draft tube (Figs. 1 and 2). The draft tube diameter was selected so that the ratio of the draft tube's internal diameter (D_{di}) to that of the internal diameter of the reactor (D_T) was 0.25. Various researchers in the past have worked with airlift reactors with various draft tube diameter to reactor diameter ratios (Kojima et al., 1999; Pironti et al., 1995). Their observation was that lower draft tube diameters to reactor diameter

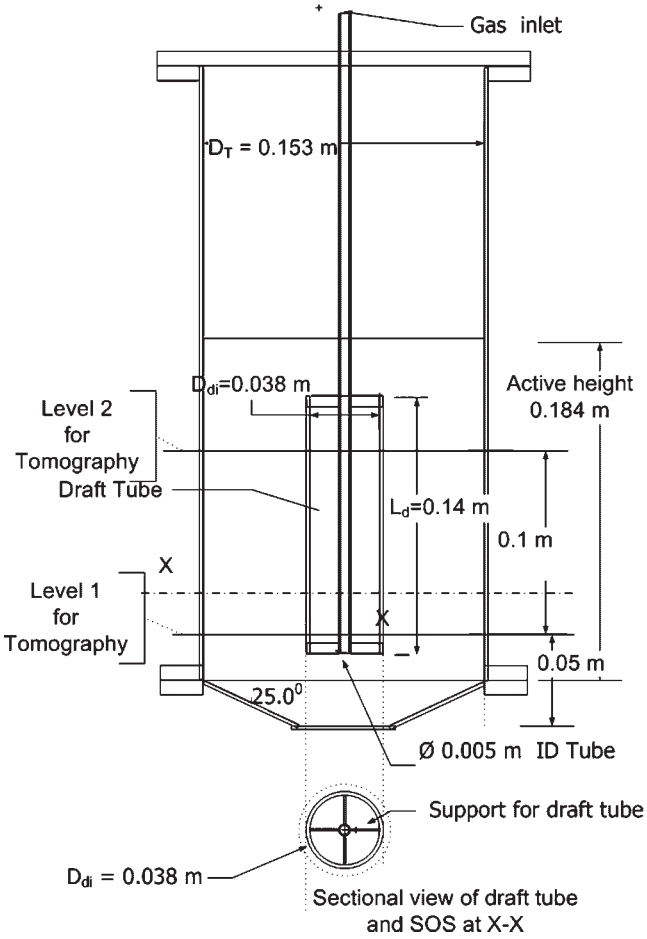

Figure 1. Cross section of the surrogate anaerobic bioreactor used with a single orifice sparger (SOS).

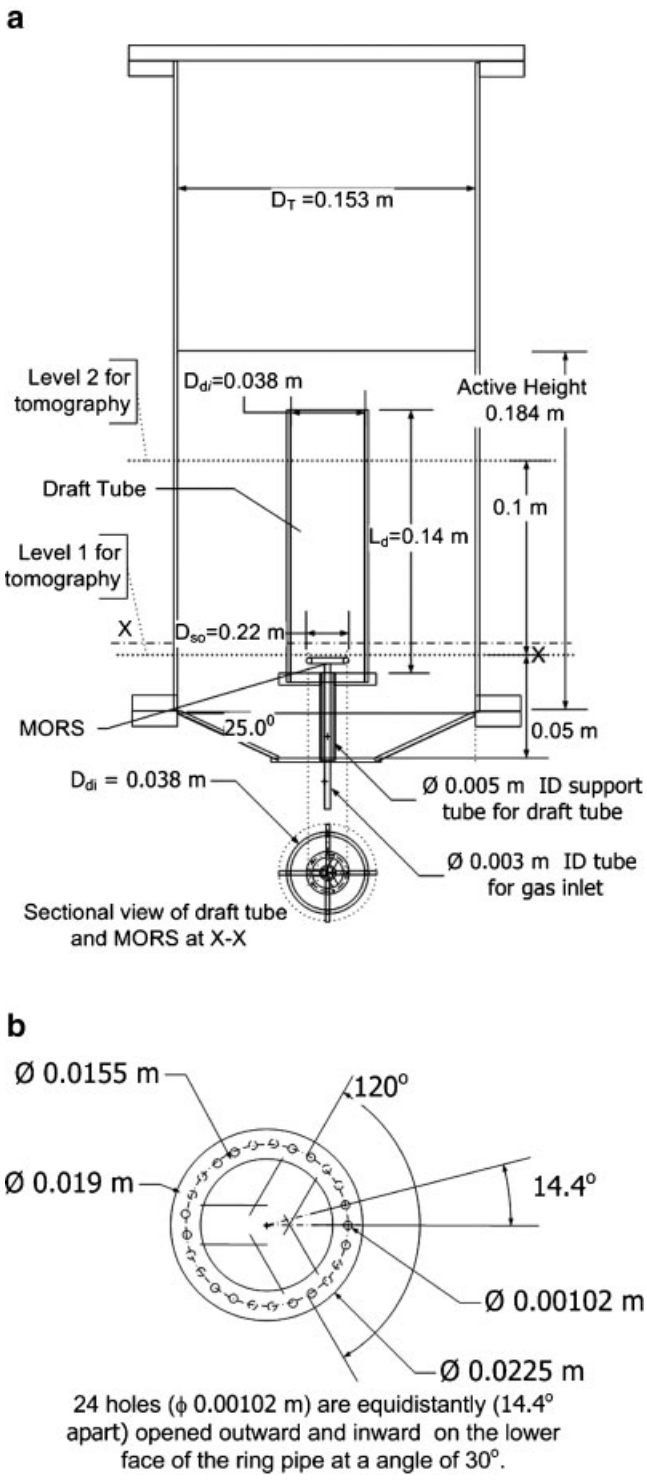

Figure 2. **a**: Cross section of the surrogate anaerobic bioreactor used a multi-orifice ring sparger (MORS). **b**: Details of the multi-orifice ring sparger (MORS) used.

ratios tend to give a higher liquid velocity in the draft tube. In a study by Karim et al. (2004) in an 8 in. (20.32×10^{-2} m) diameter gas recirculation bioreactor, the draft tube diameter to reactor diameter ratio was 0.2. Walker Process, Inc. (Aurora, IL), one of the commercial manufacturer of biogas recirculation anaerobic bioreactors for municipal wastes, makes bioreactors with ejector tubes (similar to the SOS system) with a draft tube diameter to reactor diameter ratio of 0.07–0.08. Since our aim was to study the effect of sparger design, the draft tube to reactor diameter ratio was chosen in the range of that studied by previous researchers. The draft tube was spaced equidistant from the top and the bottom of the active region of the bioreactor, along its vertical axis at the center. The effect of the conical bottom has been studied in a flow pattern visualization study, using computational fluid dynamics, by Vesvikar and Al-Dahhan (2005) for surrogate gas recirculation anaerobic bioreactors. One of the conclusions reached was that a 25° sloping angle from the horizontal gave the better performance for a given gas flow rate. Hence a conical bottom with a sloping angle of 25° from the horizontal plane was used for this study.

Single Orifice Sparger (SOS)

The SOS, as shown in Figure 1, consisted of a long 0.5×10^{-2} m i.d. steel tube which opens into the reactor at the bottom of the draft tube. The steel tube was fixed to the upper lid of the reactor. There were four flat tie rods at the upper and the lower ends of the draft tube. The rods are welded on one end to the steel tube and on the other end to the draft tube. This arrangement supported the draft tube and kept it in the desired position during operation. The gas was introduced through this tube from the top of the reactor, and it entered the reactor at the lower end of the draft tube.

Multi-Orifice Ring Sparger (MORS)

The MORS, as shown in Figure 2a, consisted of a tubular ring supplied with gas by three central tubular arms. The diameter of the orifices on the ring was 0.1021×10^{-2} m. Twenty-four equally spaced orifices were drilled in the ring (Fig. 2b). This way the open area (all orifices included) of the MORS was same as that of the SOS. The gas was introduced from the bottom of the bioreactor through a steel tube into the center of the MORS where the three cross arms meet. The MORS is set at 0.048 m from the bottom of the bioreactor. The orifices face downwards at an angle of 30° from the vertical (Fig. 2b), and face alternately inwards and outwards in pairs. The orifices open downwards to minimize the possibility of being choked or clogged with solid debris that circulates in the bioreactor slurry. Since the anaerobic bioreactor involves a gas–liquid–solid system like slurry bubble columns with fine catalyst particles, the precedent of downward facing pores in the sparger set by George et al. (2001) and Ong (2003) was followed in this case. The orifices of the MORS opened into the system at a

DOI 10.1002/bit

height of 0.042 m from the bottom of the reactor. Hence, the gas in the MORS system also entered at the same axial position as in the SOS system.

The draft tube support system consisted of four flat tie rods that connect to a flat circular strip which had an internal diameter that matches the draft tube's outer diameter. This strip was attached with fasteners (not shown in Fig. 2a) to the bottom of the draft tube. The four tie rods converged at the center, where they were welded to the wall of a steel tube. This steel tube was attached to the bottom of the reactor (at the center of the conical section) with fittings. The steel tube attached to the center of the MORS was of smaller diameter than the steel tube connected to the tie rods of the draft tube support system and was able to fit into it. This assembly was clamped to the outer tube. The gas line was attached to the tube that was connected to the MORS.

Experimental Conditions

This study used bovine manure from the University of Tennessee (UT) dairy farm at Oak Ridge, TN. The waste was pre-treated before use by wet screening through a 2×10^{-3} m sieve, followed by dilution. For this slurry the total solids (TS) level was set to 50 kg/m^3, and the volatile suspended solids (VSS) concentration was found to be 3.45 kg/m^3. A total volume of 4.2×10^{-3} m^3 for each reactor was used in the study. The gas flow rates ranged from 0.017×10^{-3} m^3/s to 0.083×10^{-3} m^3/s. Details of flow rates and the superficial gas velocity based on the draft tube diameter are given in Table I. The gas flow rate was regulated with the aid of a rota-meter attached to the airline.

Air was used in this study to substitute the biogas (a mixture of CH_4 and CO_2). Karim et al. (2005) conducted performance studies with four anaerobic bioreactors mixed by different modes processing bovine manure from the same dairy farm. One of these included a configuration similar to the SOS system. The authors reported a composition ratio of CH_4:CO_2 ranging from 56–64%:44–36% in the biogas produced. In another performance study by Borole et al. (2006) involving a gas mixed reactor with bovine manure, the ratio of CH_4:CO_2 was found to be 60:40. The molecular weight of biogas with these compositions is in the range 28.32–26.08 kg/kmol. Based on these findings air was used to substitute the biogas. Another reason for using air is that the CAPRT procedure used for liquid velocity measurement (described later) involves a calibration step that involves the insertion of a rod into the system. A hermetic system would not allow access to this calibration rod and hence would complicate the CARPT calibration process. The study by Karim et al. (2005) also indicates that the biogas generated in 24 h (once the reactor operation has reached steady state) is only about 3% of the total volume of the gas recirculated through the sparger at a rate of 0.017×10^{-3} m^3/s. Hence it can be concluded that the hydrodynamic effects due to the gas in the system are mainly caused by the recirculated biogas, and the contribution of the biogas generated by waste degradation is minimal.

The process power input into the reactor, via gas, was calculated using the expression (Eq. 1) developed by Casey (1986)

$$\frac{P}{V} = \frac{G_r P_2}{((\lambda - 1)/\lambda)} \left[\left(\frac{P_1}{P_2} \right)^{((\lambda-1)/\lambda)} - 1 \right] \quad (1)$$

P is power, V is the active volume of the reactor, G_r is the biogas recirculation rate, P_2 is the pressure in the head space, P_1 is the pressure at the point where gas in introduced (P_2 static ahead of slurry) and $\lambda = 1.03$ (Casey, 1986). The range of power input (based on gas flow rate) used in this study is within the range of 5–8 W/m^3 (summarized in Table I) suggested by the EPA (US EPA, 1979) for such systems. Therefore, it can be safely said that the surrogate anaerobic bioreactor system used in this study very closely represents a lab scale anaerobic bioreactor. Since this expression (Eq. 1) does not have terms that are dependent on the open area or other design parameters of the sparger, it is assumed that for a given gas flow rate the same amount of energy is introduced into both the systems. Hence the conclusions drawn in this study represent an actual system with a great degree of accuracy.

Overview of Computer Automated Radioactive Particle Tracking (CARPT) Technique and Experimental Procedure

CARPT is a powerful method employed for measuring the flow field, instantaneous time averaged velocities and turbulent parameters, dead zones, residence time distribution, and other parameters of a particular phase in a given system. It tracks the motion of a radioactive particle that represents an element, or small packet, of a phase in a system. It is usually used to track liquid or solid phases (Devanathan, 1991). For tracking liquids, the density of the

Table I. Flow rates conditions used and error in CARPT calibration process for anaerobic bioreactor with SOS and MORS systems.

Gas flow rate $Q_g \times 10^3$ (m^3/s)	Superficial gas velocity based on draft tube diameter $\times 10^3$ (m/s)	Superficial gas velocity based on reactor diameter $\times 10^3$ (m/s)	Power input (W/m^3)	Average calibration error for reactor with MORS $\times 10^3$ (standard deviation $\times 10^3$) m	Average calibration error for reactor with SOS $\times 10^3$ (standard deviation $\times 10^3$) m
0.017	1.47	0.09	8.71	0.26 (0.14)	0.37 (0.21)
0.050	4.41	0.27	26.15	0.37 (0.24)	0.38 (0.19)
0.083	7.35	0.45	43.58	0.31 (0.17)	0.39 (0.23)

radioactive particle (usually a few hundred microns in size) is made to match the density of the liquid by encapsulation in a polypropylene (PP) ball. Such a particle is tracked with the aid of an array of NaI scintillation detectors placed at strategic locations around the system. A typical CARPT study involves the following sequence of steps: preparation of radioactive particle, in situ calibration (at experimental conditions), experimental runs, and processing of the data generated from the preceding two steps (Roy, 2000). These aspects have been discussed in brief here to maintain continuity, for further details the reader is advised to refer to the works of Karim et al. (2004), Devanathan (1991), and Degaleesan (1997).

Particle Preparation

In this study, the liquid phase was tracked. A ^{46}Sc radioactive particle of 300 μCi strength and 150 μm diameter was encapsulated in a PP ball of 0.001 m diameter with a calculated air gap. The density of the composite particle was made to match that of water. This was done by determining the density of the composite particle based on its terminal settling velocity and Stoke's law (Eq. 2)

$$U_t = \frac{gD_p(\rho_p - \rho_W)}{18\mu_W} \tag{2}$$

To determine the settling velocity the particle was released in a 1 m long acrylic tube filled with water. The terminal settling velocity was calculated based on the time taken to settle in the last 0.5 m of the tube. Then using Equation (2), its density was calculated. If the particle was light, it was coated with commercial spray paint to make it heavy. If it was heavy, it was made lighter by coating it with a commercial epoxy glue spray with a density less than that of water. After repeated adjustments the composite particle used for the experiments had a density of 1.0016 kg/m^3 (average absolute error = 0.0016, standard deviation = 0.0012: based on five terminal settling velocity measurements).

Calibration, Particle Tracking, and Data Processing

The gamma ray photon counts received by the NaI scintillation detectors are a function of the distance of the radioactive particle from the detector, and of the attenuation of the photons due to the material between the detector and particle. Hence the calibration process is carried out in situ, that is, the reactor was operating at the given conditions and configuration for which the experiment was to be carried. Thus, the number of counts received during calibration matches the counts received if the free particle were to be at the same location in the tracking experiment (described later). For a given signal strength (or the number of counts) detected for a particular detector, the particle could be anywhere along the surface of a hypothetical sphere with a radius represented by the distance the corresponding counts or signal strength refer to. Hence a minimum of three detectors are required to pinpoint the location of a particle. A total of 16 detectors were used in this system. In this study, an automated calibration device developed by Luo (2005) was used.

To test for error in the calibration, the counts data for the known positions of the particle was split into two groups, which constitute 80% and 20% of the complete data set. The 80% data set was used to calibrate the system by developing a distance-counts map. The 20% data set was traced based on this distance count map. The traced positions were compared to the positions (distance) at which these data points (the 20% set) were taken. Error was determined by taking the mean of the differences in the position. The results summarized in columns 5 and 6 in Table I show that the average error was 0.003 m.

Once the calibration procedure was completed the particle was removed from the calibration rod and introduced into the system. The particle was allowed to move freely within the system, unhindered by external influence. While the particle was moving in the reactor operating at the set conditions, the counts received by all the detectors were recorded at the same sampling rate as it was calibrated (in this case, 50 Hz). This tracking process was carried out for 18 h for all the conditions described in Table I, which provides enough data to reach asymptotic values of time averaged velocity for each location in the system.

To reconstruct the position of particle based on the tracking data, the distance-count map generated by the calibration process was used. Each location of the particle was at a time interval of 0.02 s; hence the instantaneous position (i.e., Lagrangian trajectory) of the particle was obtained. The process involves the application of a weighted least-squares algorithm; a wavelet-based position filtering, and by a particle position reconstruction algorithm described elsewhere (Degaleesan, 1997; Devanathan, 1991; Rados, 2003). Time differencing between two positions yielded instantaneous velocities, which were averaged at each spatial location over the whole time span of the experiment to yield the ensemble average velocity flow map of the system. To get Eulerian information, the volume of the reactor was divided into 28,160 cells (20 divisions in r, 32 in θ, and 44 in the z direction, respectively). This enables better resolution in visualizing the velocity profile. The number of cells used is determined on the basis of work done by Degaleesan (1997). The estimated instantaneous velocity information was then assigned to the cell falling at the midpoint of two successive particle positions. The average liquid velocity data thus generated were used for comparison in this study.

Overview of Computer Tomography (CT) Technique and Experimental Procedure

Data Acquisition Process

The details of the of the mechanical hardware and the data acquisition system for the single source γ-ray CT unit used

DOI 10.1002/bit

in this study has been described at length by Karim et al. (2004) and Roy (2006). The E-M algorithm proposed by Lange and Carson (1984) and implemented by Kumar (1994) was used for image reconstruction.

CT Data Processing

Single source CT can be used to compute the individual phase holdup of only a two phase system, and can be extended to three phases where one of the phases is stationary, like the solid phase in a column with structured packing (Roy et al., 2004). In this study, the liquid and solids were considered as a single slurry phase, as the solids concentration was only 5% (w/v basis), and the solids contribution to attenuation was minimal. Also, the pretreatment avoided large debris and sand particles, etc., in the system that would cause high attenuation. Per Beer-Lambert's law, the attenuation by any substance is a linear sum of the attenuation of the individual pure components. Therefore, the attenuation value computed for a given pixel in the image domain via the process of tomography by the use of the E-M algorithm is a liner sum of the attenuation of the pure components in the pixel (Eq. 3)

$$\mu_{\mathrm{EM},l-\mathrm{g}}\langle x\rangle = \mu_l \varepsilon_l\langle x\rangle + \mu_{\mathrm{g}}\varepsilon_{\mathrm{g}}\langle x\rangle \tag{3}$$

Additionally, because of the fact that the system consists of only two phases, gas and slurry, the sum of the volumetric fractions of these two phases is unity (Eq. 4) for any given pixel. The pure component values are usually available from literature. However, in this case, for accuracy the reactor was scanned with the individual phases, that is, empty (with air) and with the slurry. The scans for such systems are represented by Equations (5) and (6), where the values of the holdups are unity.

$$\varepsilon_l\langle x\rangle + \varepsilon_{\mathrm{g}}\langle x\rangle = 1 \tag{4}$$

$$\mu_{\mathrm{EM,g}}\langle x\rangle = \mu_l \varepsilon_l^o\langle x\rangle \tag{5}$$

$$\mu_{\mathrm{EM,g}}\langle x\rangle = \mu_{\mathrm{g}} \varepsilon_{\mathrm{g}}^o\langle x\rangle \tag{6}$$

$$\varepsilon_l^o\langle x\rangle = \varepsilon_{\mathrm{g}}^o\langle x\rangle = 1 \tag{7}$$

Hence, the holdup of the gas phase can be calculated based on Equation (8), which is derived from Equations (3–7)

$$\varepsilon_{\mathrm{g}}\langle x\rangle = 1 - \left(\frac{\mu_{\mathrm{EM},l-\mathrm{g}}\langle x\rangle - \mu_{\mathrm{EM,g}}\langle x\rangle}{\mu_{\mathrm{EM},l}\langle x\rangle - \mu_{\mathrm{EM,g}}\langle x\rangle}\right) \tag{8}$$

Scans of the systems with SOS and MORS were carried out at level 1 (5×10^{-2} m from the base of the reactor) and at level 2 (15×10^{-2} m from the base of the reactor) as indicated in Figures 1 and 2, respectively.

Results and Discussion

Computed Tomography

Effect of Gas Flow Rate and Sparger Configuration on Gas Holdup Distribution

Figure 3 shows a three-dimensional perspective of the tomograms showing the time averaged gas holdup

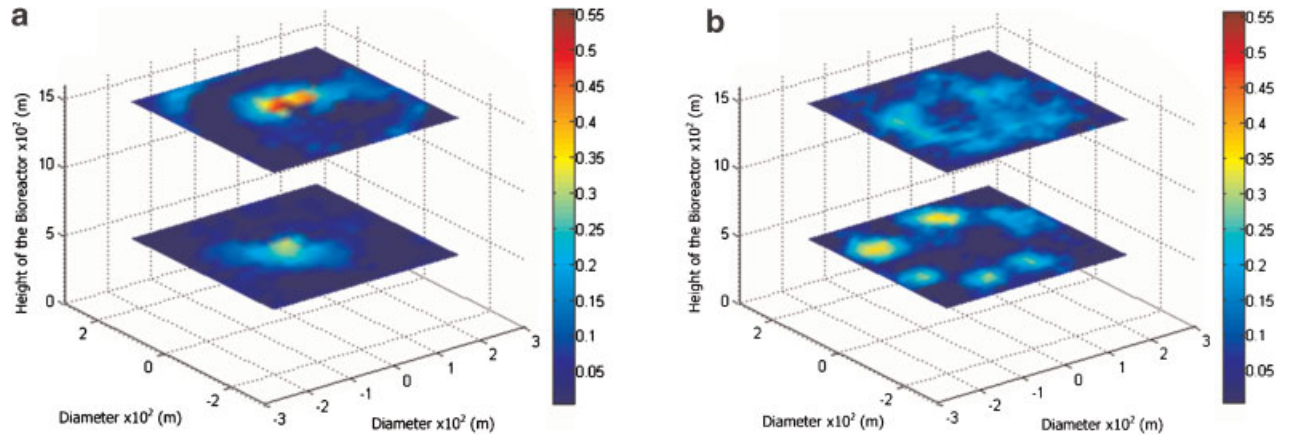

Figure 3. Three-dimensional representation of tomograms showing cross sectional time averaged gas holdup distribution in the draft tube region for (**a**) system with SOS and (**b**) system with MORS at level 1 (5×10^{-2} m) and level 2 (15×10^{-2} m) at $Q_g = 0.05 \times 10^{-3}$ m^3/s (superficial draft tube gas velocity $= 4.41 \times 10^{-2}$ m/s). Color bar represents the holdup value. [Color figure can be seen in the online version of this article, available at www.interscience.wiley.com.]

distribution of the system with the SOS and the MORS, at levels 1 and 2 in the draft tube region with a gas flow rate of 0.05×10^{-3} m^3/s. These images have been reconstructed on the basis of Equation (8). The draft tube region alone has been shown here as the tomograms generated for the entire cross section (not sown here) show that gas holdup in the region outside the draft tube in the reactor is negligible. This can be seen in Figures 5 and 6 which shows the radial gas holdup profile (discussed later). The gas spreads within the draft tube as it is released and rises in the draft tube for both the systems. The MORS system has more gas distributed in the draft tube than does the SOS. In Figure 3a there is a local spot of high gas holdup visible at the center within the SOS system at level 2 (15×10^{-2} m from the base of the reactor). This represents the gas inside SOS injector tube that extends from the top of the reactor to the bottom region of the draft tube (Fig. 1). There is also a concentration of the gas phase near the center of the draft tube surrounding the SOS injection tube. This shows that there is certain degree of channeling of the gas within the central region of the draft tube in the reactor with the SOS system, as it rises within the draft tube after it is introduced at the bottom of the draft tube.

The gas holdup distribution in the draft tube of the MORS system is quite different. The gas holdup is confined to circles over the ring sparger at level 1 (0.05 m from the base), as level 1 is located very close to the MORS. The gas then distributes itself over the region of the draft tube for the system with MORS as it rises, as seen in at level 2 in Figure 3b. For both the SOS and the MORS, the gas flow rates were maintained at 0.05×10^{-3} m^3/s in Figure 3, hence a better gas holdup distribution is observed in the draft tube region of the bioreactor with MORS.

The presence of the local circular regions of gas holdup above the sparger also indicates that for the given flow rate not all the pores in the MORS open up. At a higher gas flow rate (0.082×10^{-3} m^3/s), more open pores are observed in the tomogram as shown in Figure 4. There is insufficient pressure drop across the sparger at lower flow rates to open all the pores in the sparger. The gas holdup tomograms do not have resolution high enough to judge the exact number of open pores in the MORS. It must be noted that even with a few pores open at low gas flow rates, the MORS still gives a better gas holdup distribution than the SOS.

An alternative, to ensure all pores open, could be to reduce the diameter of the pores further (and there by reducing the open area) with out compromising the number of pores. However, given the nature of the bovine manure slurry and its inconsistency in terms of the characteristic of the solids present in it, the chances of pore clogging would be high during operation for very small pores. The other alternative could be to reduce the number of pores in the sparger such that the minimal gas flow rate covered in the study would open all the pores. This in turn could reduce the number of pores drastically (depending on the gas flow rate it would be designed for). When this design (with reduced number of pores) is used for higher flow rates the

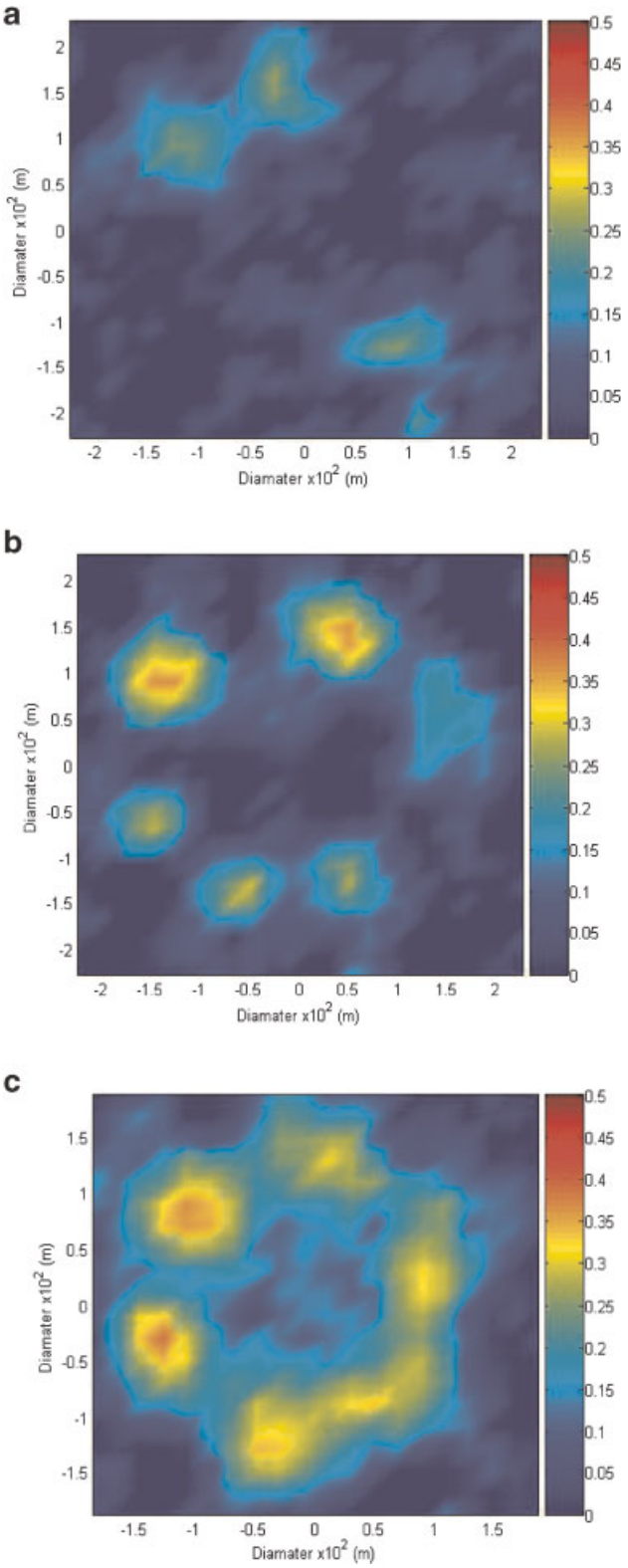

Figure 4. Tomograms of system with MORS at level 1 with gas flow rates (**a**) 0.017×10^{-3} m^3/s, (**b**) 0.05×10^{-3} m^3/s, and (**c**) 0.083×10^{-3} m^3/s. [Color figure can be seen in the online version of this article, available at www.interscience.wiley.com.]

DOI 10.1002/bit

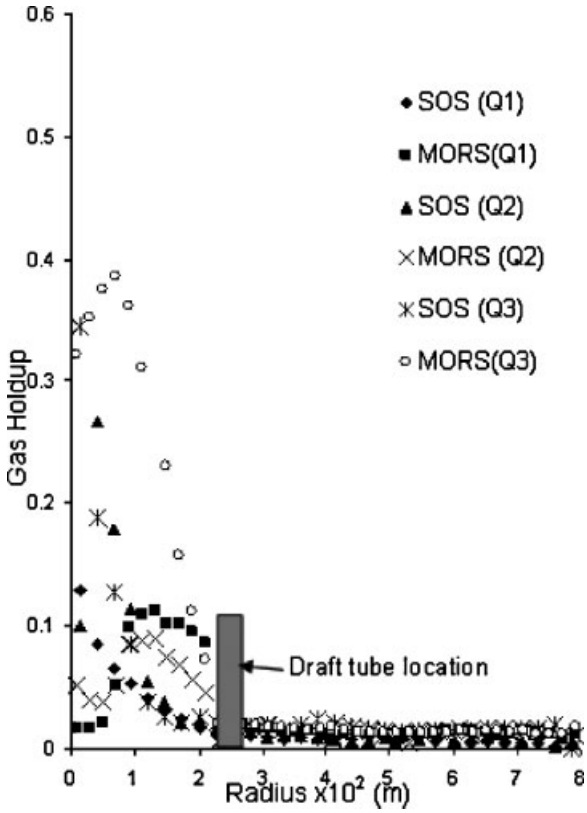

Figure 5. Comparison of azimuthally averaged gas holdup profiles for system with SOS and system with MORS at level 1 for different flow rates (indicated in parenthesis $Q1 = 0.017 \times 10^{-3}$ m^3/s, $Q2 = 0.050 \times 10^{-3}$ m^3/s, and $Q3 = 0.083 \times 10^{-3}$ m^3/s).

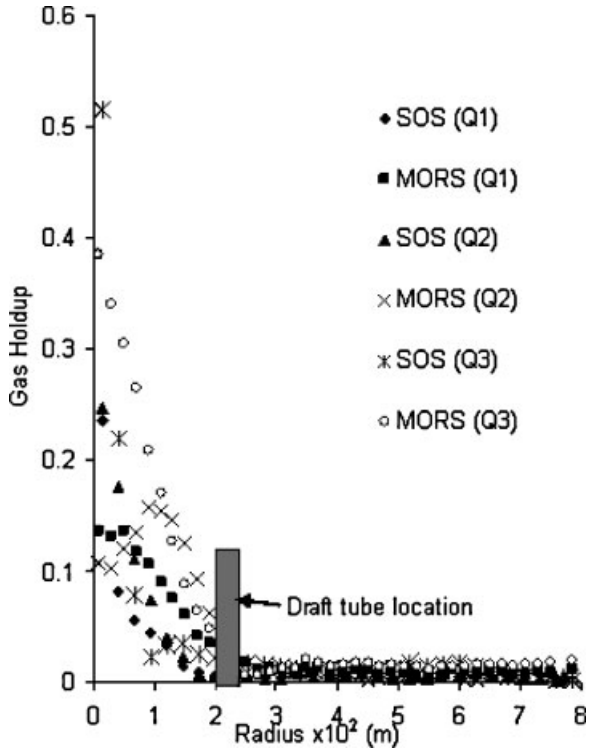

Figure 6. Comparison of azimuthally averaged gas holdup profiles for system with SOS and system with MORS at level 2 for different flow rates (indicated in parenthesis $Q1 = 0.017 \times 10^{-3}$ m^3/s, $Q2 = 0.050 \times 10^{-3}$ m^3/s, and $Q3 = 0.083 \times 10^{-3}$ m^3/s).

hold up distribution would be affected as the gas would be confined to limited number of pores versus a scenario where it could have been introduced through a higher number of pores, there by giving better gas holdup distribution. For this study, having a different sparger for each of the gas flow rates with specific number of pores (such that all are open during operation) would have been impractical.

Figures 5 and 6 depict the azimuthally averaged mean gas holdup profiles in the reactor at levels 1 and 2 respectively, where the gas holdup is plotted versus radius. The values for all the flow conditions covered in Table I are shown for both SOS and MORS systems. It is clearly visible that at level 1 (Fig. 5) for the case of the SOS there are certain local spots where the gas holdup is higher than that of the MORS for a given gas flow rate. The local peak (at a radius of 1×10^{-2} m) in the gas holdup profiles of the MORS is due to the fact that the location of level 1 is just above the MORS; hence the gas coming out the orifice is responsible for this peak. At level 2 (Fig. 6), the gas holdup distribution is more radially uniform in the MORS system. In contrast, all the profiles for the SOS system show a distinct peak near the center of the reactor. A better understanding can be obtained by observing the mean of the gas holdup profile. Figure 7 shows the mean gas holdup in the draft tube versus the superficial gas flow velocity. The superficial gas velocity is based on the gas flow rate and the cross-sectional area of the draft tube. The mean gas holdup is calculated by Equation (9)

$$\overline{\varepsilon_g} = \frac{\sum_{x=1}^{n_{draft}} \varepsilon_g \langle x \rangle}{n_{draft}} \tag{9}$$

Here x represents the pixel index, and n_{draft} the number of pixels in the draft tube region. Since the area each pixel represented in the domain is equal, $\overline{\varepsilon_g}$ in Equation (9) is an area weighted average gas holdup.

Figure 7 clearly confirms that the mean gas holdup is higher for the MORS system at both levels 1 and 2. As gas flow rate increases, the gas holdup increases. This rise in gas holdup with gas velocity is more pronounced in the case of the MORS system. The superficial velocities' effect on gas holdup is well known. However, what is highlighted here is that the effect sparger design and its impact on gas holdup distribution. For a fixed superficial gas velocity the system with MORS gives a higher (spatially) average gas holdup in the draft tube. The impact of this enhancement in gas holdup distribution on the liquid velocity and poorly mixed zones outside the draft tube will be discussed in the CARPT results section.

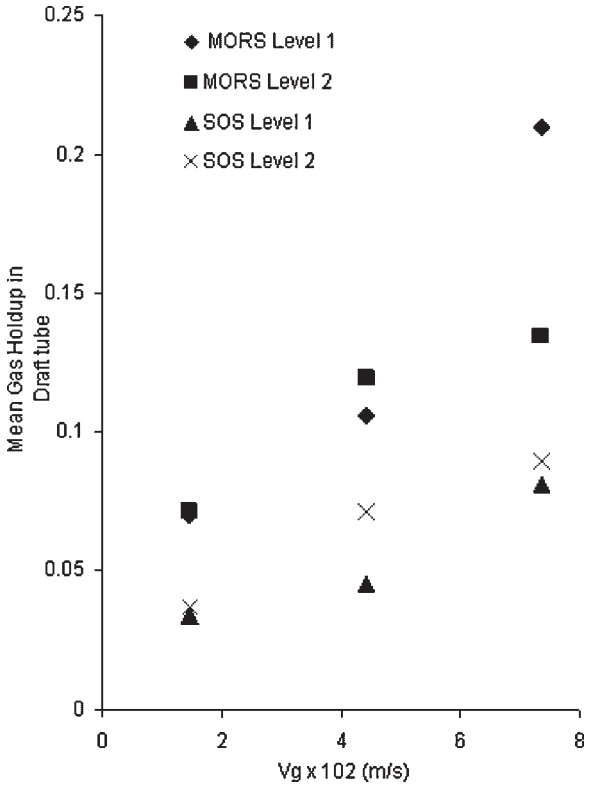

Figure 7. Mean gas holdup in the draft tube region of the SOS and MORS systems at levels 1 and 2.

Characterization of the Uniformity of Gas Holdup Distribution

It is important to quantify the uniformity of the cross-sectional gas holdup distribution in order to properly compare the effects of the design and operation parameters of the bioreactor. In this section the different approaches have been discussed with their merits and demerits.

Maldistribution in flows, particularly those that contain liquids, has been characterized at length in the literature. Some of these approaches divide the domain of flow into sub-domains of a given size. Then statistical tools are used to compare the holdup in this sub-domain with the global mean (i.e., mean of the entire domain). Marcandelli et al. (2000) calculated the maldistribution factor for liquid flow in gas–liquid packed columns using Equation (10). The flow domain was divided into nine sectors (denoted by N)

$$M_f = \sqrt{\frac{1}{N(N-1)}\sum_{n=1}^{N}\left(\frac{\varepsilon_{l,n}-\overline{\varepsilon_l}}{\overline{\varepsilon_l}}\right)} \qquad (10)$$

Here M_f is the maldistribution factor, $\overline{\varepsilon_l}$ is the mean liquid holdup (based on the entire domain) and $\varepsilon_{l,n}$ is the sub-domain gas holdup. Roy (2006) has used a t-test-based method on liquid saturation data in packed monolith reactors obtained from computed tomography (CT). In this approach the main domain was divided into several sub-domains of 6 pixels each. Each of these sub-domains was compared with a hypothetical sub-domain of the same size (6 pixels) that has the mean holdup values calculated based on the entire domain (global mean), with the aid of the t-test with a 95% confidence interval. If the sub-domain "passed" the t-test, the null hypothesis was satisfied, the two groups were statistically the same, and the value 1 was assigned to that sub-domain group. If it failed then a 0 was assigned. Finally a uniformity factor was determined as a percentage of the sum of domains labeled with 1. The sub-domain t-test has the right conceptual fundamentals and is able to give a quantitative value to degree of uniformity in terms of a percentage, which is convenient for the purpose of comparison.

However, domain-based methods in general have the two drawbacks. The first drawback is the strategy one uses for choosing the size and orientation of the sub-domain. Experimentalists who use collectors to make liquid distribution measurements in structured columns typically create sub-domains in the collectors in the order of 16–25 in number, and hence find it convenient to use a sub-domain oriented strategy. Since the orientation of the sub remains constant in the setup, liquid flow distribution with different packing materials and operational conditions can be compared. However if one were to vary the sub-domain size, the results differ. The second drawback is the problem that could evolve in situations where the holdup of the particular phase of interest is small and confined to a small region. While computing the mean holdup of the entire domain in order to carry out the t-test, the weighted contribution of the holdup to all the pixels, from the few that have the phase in them, may be very small. When the t-test is done there would not be any statically significant difference in the mean of the sub-domain and the global mean. Hence the analysis would indicate that the system is very well distributed, which would be counter intuitive to the visual observation in the tomogram.

To take a better look at the effect of the domain size on the gas holdup distribution, the MORS system data at 0.05×10^{-3} m^3/s gas flow rate at level 2 was subjected to the t-test-based uniformity factor analysis using the Roy (2006) approach. There are 436 pixels in the domain representing the cross-section of the draft tube. Sub-domains with pixels blocks varying from 5 to 50 were used yielding results shown in Figure 8. Clearly the distribution factor varies as the size of the domain changes. There is no asymptote visible in Figure 8, even where small numbers of pixels are used for a sub-domain, which would make the number of sub-domains large. However, if the holdup distribution analysis is performed for different flow conditions in a given experimental setup then one fixed sub-domain size may be considered as a basis for comparison. This type of analysis would not inspire confidence in characterizing holdup distribution in a system for universal comparison.

The t-test-based analysis was carried out for this study, using a sub-domain size of 6 pixels. The results

DOI 10.1002/bit

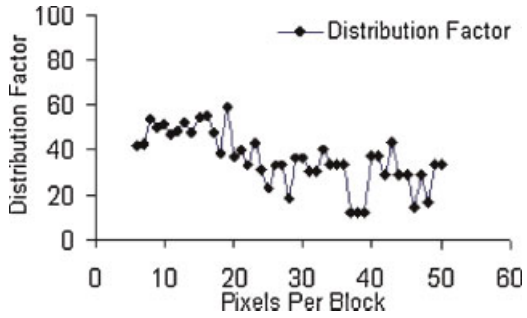

Figure 8. Plot showing dependency of distribution factor on number of pixel per block used for computing distribution factor based on *t*-test. Gas holdup distribution data from the scan at level 2 for the MORS system with $Q_g = 0.05 \times 10^{-3}$ m^3/s was used.

are summarized here. For $V_g = 1.46 \times 10^{-2}$ m/s ($Q_g = 0.017 \times 10^{-3}$ m^3/s), at both levels 1 and 2 the uniformity factor for the MORS system is a little more than double as that of the SOS (level 1: MORS = 61.0%, SOS = 27.8%; level 2: MORS = 53.2%, SOS = 30.5%) system. There is a similar trend for $V_g = 4.41 \times 10^{-2}$ m/s ($Q_g = 0.05 \times 10^{-3}$ m^3/s) at both levels (level 1: MORS = 42.5%, SOS = 21.1%; level 2: MORS = 51.0%, SOS = 33.3%). However, when compared to the previous flow rate, the uniformity factor values appear to be lowered. Finally for $V_g = 7.35 \times 10^{-2}$ m/s ($Q_g = 0.083 \times 10^{-3}$ m^3/s), the values for distribution at levels 1 and 2 are almost comparable for the MORS and SOS systems (level 1: MORS = 36.2%, SOS = 23.2%; level 2: MORS = 21.0%, SOS = 21.3%). These observations are contrary to tomograms for these levels (not shown) and the azimuthally averaged gas holdup profiles shown in Figures 5 and 6.

A simpler statistical method is developed in this work where the variance of the holdup distribution of the entire domain is calculated based on the gas holdup in each pixel in the domain. The variance is normalized by the mean gas holdup for that domain. This non-dimensional variance (Eq. 11) can be called a maldistribution factor. This equation bears resemblance to the ones used by Marcandelli et al. (2000) and Jiang (2000) to characterize maldistribution

$$\sigma = N_{\mathrm{Mal}} = \sqrt{\frac{1}{n}\sum_{j=1}^{n}\left(\frac{\varepsilon_{g,j}\langle x\rangle - \overline{\varepsilon_g}}{\overline{\varepsilon_g}}\right)^2} \qquad (11)$$

If the variance of the holdup data is zero, this would indicate that holdup profile is absolutely uniform and even (maldistribution is zero). If non-dimensional variance tends towards unity, it is maldistributed. One must be aware that this value could be greater than unity in severely maldistributed cases.

It is therefore better to call this ratio a "maldistribution number (N_{Mal})," just like any non-dimensional number, as factors or coefficients tend to be between zero and unity. This method is more simple and fundamental and not dependent on the size or geometrical orientation of the subdomains involved. Also, as the number of pixels (n in Eq. 11) increases, by statistical principles the accuracy of N_{Mal} will also increase.

N_{Mal} values based on Equation (11) are shown in Figure 9. It should be noted that the smaller the N_{Mal} value, the better the gas holdup distribution. Clearly, for $V_g = 1.46 \times 10^{-2}$ m/s ($Q_g = 0.083 \times 10^{-3}$ m^3/s) there is difference in N_{Mal} by a factor of 2 (over 100% difference) at level 2 for the SOS and MORS systems. This difference is also seen at $V_g = 4.41 \times 10^{-2}$ m/s ($Q_g = 0.05 \times 10^{-3}$ m^3/s). At higher V_g values, this difference narrows a bit, but still differs by a factor of 70–80% between the SOS and MORS systems. All the N_{Mal} values for SOS are above unity, this indicates severe maldistribution of the gas in the draft tube region for the system with SOS. Hence it can be concluded that the MORS, in spite of partially opened pores (Fig. 4), gives a better gas holdup distribution than the SOS for a given gas flow rate.

Results From Computer Automated Particle Tracking (CARPT)

Liquid Velocity and Flow Pattern in Digester With MORS and SOS

Selected results of the azimuthally average mean liquid velocity values computed from the CARPT data are represented in the quiver plots in Figure 10. This figure

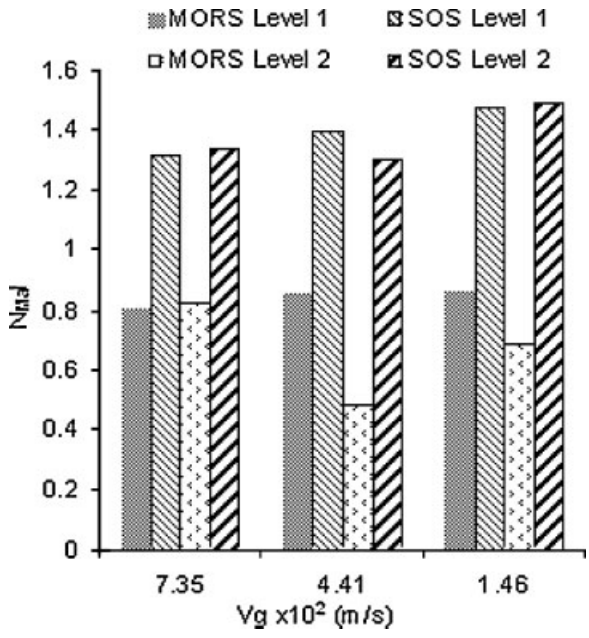

Figure 9. Normalized standard deviation or maldistribution number (N_{Mal}) based comparison for gas phase distribution in the draft tube region for a SOS system and MORS system.

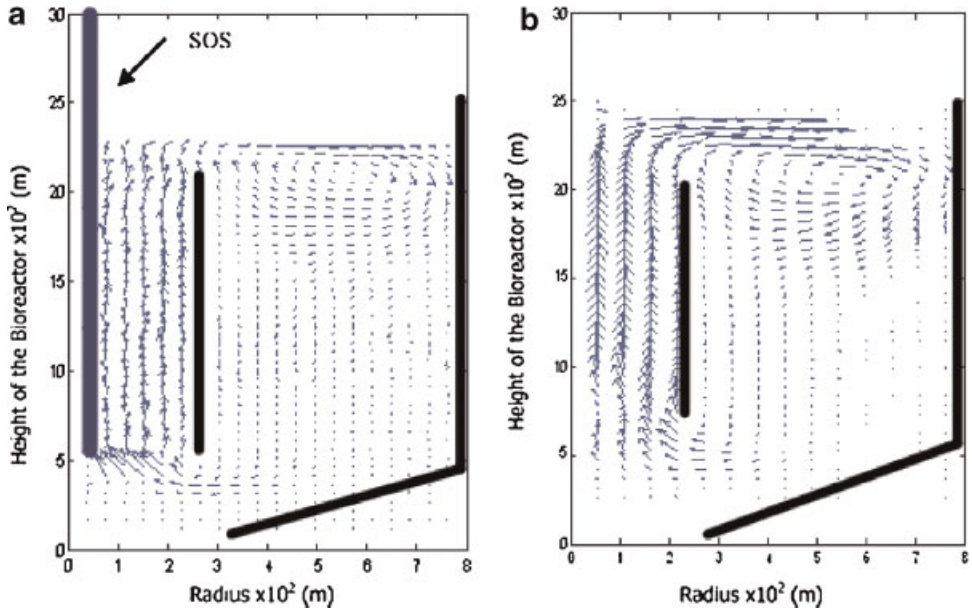

Figure 10. Time averaged velocity vector plots for digester with 5% (TS) solid loading slurry at for gas flow rate $Q_g = 0.05 \times 10^{-3}$ m^3/s ($V_g = 4.4 \times 10^{-2}$ m/s): (**a**) SOS, (**b**) MORS. The dark lines indicate the location of the wall of the reactor and the draft tube. [Color figure can be seen in the online version of this article, available at www.interscience.wiley.com.]

depicts the azimuthally averaged velocity vectors in the system formed due to its axial and radial components, hence depicting the flow pattern in the digester with the MORS and SOS systems (for $Q_g = 0.05 \times 10^{-3}$ m^3/s and $V_g = 4.4 \times 10^{-2}$ m/s in draft tube). As mentioned earlier, the system is divided into small cells for data processing; the vectors in this figure are shown for each such cell. It can be observed that two circulation loops exist. The liquid tends to rush into the bottom part of the draft tube in the region where the gas is introduced through the sparger, as is evident for both the MORS and the SOS system. It can be observed in this region that the velocity vectors are more prominent in the SOS system (Fig. 10b). By virtue of the design of the SOS system, the gas is introduced at one single location into the system, which creates a local low density spot which sucks the liquid into this region. The liquid then is carried up the draft tube and gets released in the upper section of the reactor. The streamlines plot shown in Figure 13 depict the direction of flow liquid in the system, these confirm the results shown in Figure 10 for the SOS and MORS system.

Similar observations were made by Karim et al. (2004). Gas in the draft tube facilitates this process. With the momentum gained, the liquid is then pushed to the periphery of the reactor, as evident from the high radial component of the velocity vector in the upper part of the bioreactor (Fig. 10). The liquid is then pulled back into the region around the exterior of the draft tube after it comes in contact with the wall of the reactor. Hence a recirculation eye is formed in the upper part of the reactor around the draft tube region, which suggests that the entire peripheral region of the reactor does not act as a downcomer. The velocity vectors are more uniform in the draft tube region for the MORS system, as they have a stronger axial component than in the SOS system. This suggests that the stream of gas bubbles tends to spiral around in the region between the SOS and the draft tube; hence there is a significant radial component which prevents the arrows from being vertically oriented (Fig. 10b). This phenomenon does not arise in the MORS system, as a better gas holdup distribution essentially reduces the radial components in the velocity vectors. Hence the flow is uniform in MORS as the arrows appear pointed upwards (Fig. 10a). The flow pattern trends observed in the quiver plots are similar for both spargers to those observed in Figure 10 for other flow conditions (listed in Table I), and hence they are not shown here.

Axial Liquid Velocity

Figures 11 and 12 show the plot of the azimuthally averaged mean axial liquid velocity versus the radius of the system. These figures help visualize the values in quantitative terms. It can be seen that the axial velocities in the system with MORS are higher than that with SOS system for any given gas flow rate at both levels 1 and 2. This is attributed to the higher mean gas holdup, as seen in Figure 7, and better gas distribution in the draft tube due to the lower values of N_{Mal} (Fig. 9) for the MORS system. The liquid velocities are higher at level 2 for any given sparger and gas flow rate. This is attributed to the fact that the gas distribution is better at level 2 for any given gas flow rate and sparger. The higher liquid velocity in the draft tube creates more circulation in

DOI 10.1002/bit

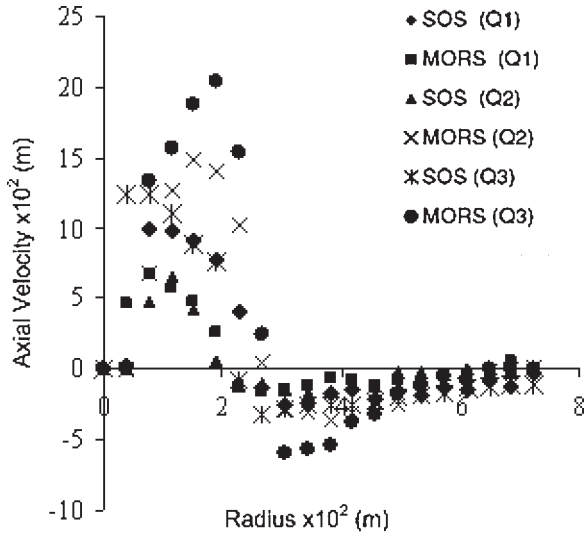

Figure 11. Time averaged axial velocity comparison for level 1 (5×10^{-2} m) from CARPT data. The gas flow rates have been indicated in parenthesis ($Q1 = 0.017 \times 10^{-3}$ m^3/s, $Q2 = 0.050 \times 10^{-3}$ m^3/s, and $Q3 = 0.083 \times 10^{-3}$ m^3/s).

the downcomer region, as can be seen in the increase in the negative axial velocity in the downcomer region of the reactor for higher gas flow rates. This increase is an indication of better circulation in the system.

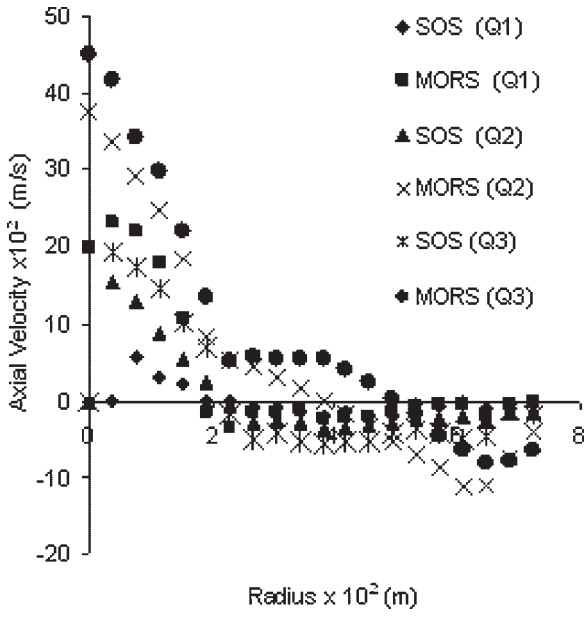

Figure 12. Time averaged axial velocity comparison for level 2 (150×10^{-2} m) from CARPT data. The gas flow rates have been indicated in parenthesis ($Q1 = 0.017 \times 10^{-3}$ m^3/s, $Q2 = 0.050 \times 10^{-3}$ m^3/s, and $Q3 = 0.083 \times 10^{-3}$ m^3/s).

Determining Poorly Mixed Zones and Root Mean Square (RMS) Liquid Velocity

To better understand the effect of the sparger configuration on the mixing in the bioreactor a contour plot of root mean square (RMS) values of the radial, azimuthal, and axial time averaged components of the velocity was prepared. The velocity contours help identify the zones in the system where the liquid velocity is such that it would cause the solids or bio flocs in the slurry to settle. Unfortunately, since the data for bio flocs settling characteristics of the slurry used in this study was not gathered during the experiments, the settling values available in literature were used to mark these contours. The terminal settling velocities for flocs from similar systems are reported in the range of 0.2×10^{-3} m/s to 20×10^{-3} m/s (Lee et al. 1996; Li and Yuan, 2002). Based on Li and Yuan (2002), Karim and Thoma (2007) have used a settling velocity of 0.32×10^{-2} m/s as a criteria for determining poorly mixed zones in gas-lift digesters. This same liquid velocity value has been used here to develop a slice of the velocity contours along the radial and axial direction of the bioreactor as shown in Figure 13 for one of the gas flow rate condition studied. The regions of the reactor that has liquid velocity below the contour with a velocity 0.32×10^{-2} m/s have been indicated in the darkest shade. This figure also depicts the streamline in the system generated from the velocity data obtained from the CARPT experiments using the *streamline slice* function available with Matlab® software. The streamlines clearly depict the circulation patterns observed in the bioreactor. The bottom part of the system with SOS shows zones with no streamlines indicating negligible liquid velocity. Some breaks appear in the streamlines in Figure 13. These could be due to the experimental error associated with the CAPRT technique and the fact that a two-dimensional plane (r–z slice) for a given value of θ ($\theta = 0^0$) is depicted. Hence, the broken streamlines are the ones that enter and leave this plane. The contour plots show greater fraction of the volume of the reactor under the velocity contour for 0.32×10^{-2} m/s in the system with SOS. Table II summarizes the volumetric percentage of poorly mixed zones in the reactor for all the gas flow rates covered for both the system based on the three-dimensional (r, θ, and z) contour plots developed (not shown). These results clearly show that the poorly mixed zones double when a SOS system is used for a given gas flow rate. For the higher superficial gas velocity covered, the MORS reduces the poorly mixed zones by a factor of three. This is because the MORS system has lower N_{Mal} value in the drat tube region for a given flow rate, this creates a higher density gradient between the draft tube region and the outside region within the reactor that increases the liquid circulation. The presence of poorly mixed zones would over a period of time encourage the settling of solids in the reactor which could lead to the drop in performance of the system. Since these types of reactors have a high hydraulic retention time, over a period of time the system with SOS is likely to accumulate a lot of solids as compared to MORS.

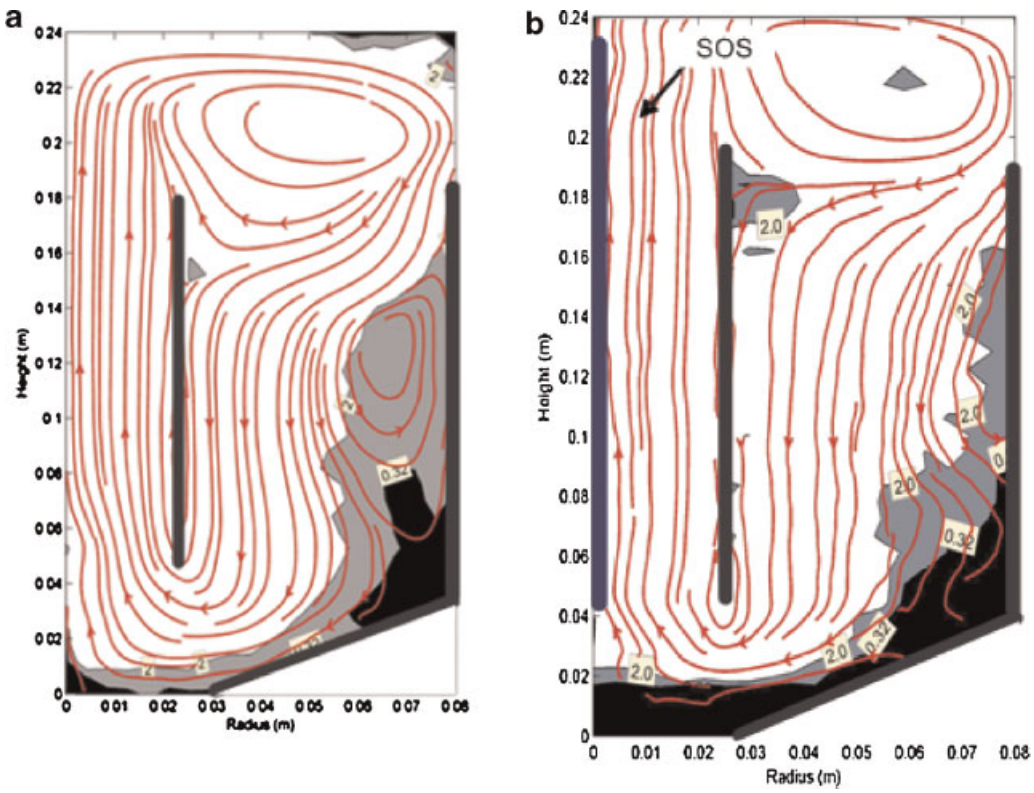

Figure 13. Contour plots showing the time averaged values of the magnitude of the liquid circulation velocity for the bioreactor with 5% (TS) solid loading slurry at for gas flow rate $Q_g = 0.05 \times 10^{-3}$ m^3/s ($V_g = 4.4 \times 10^{-2}$ m/s): (**a**) MORS, (**b**) SOS. The dark lines indicate the location of the wall of the reactor and the draft tube; the fine lines with arrows indicate the streamlines. Numeric values in the box indicate velocity $\times 10^2$ (m/s) values the contour represents. The black colored zones indicate poorly mixed regions. [Color figure can be seen in the online version of this article, available at www.interscience.wiley.com.]

The mean per cell, time averaged RMS velocity values obtained from all the cells in the draft tube region and the all the cells in the reactor (including draft tube region) for the reactor with MORS and SOS give an idea of the impact of gas flow rate on the liquid velocity. The mean time averaged RMS velocity for the draft tube region alone, as well as the entire reactor, is shown for the different superficial gas velocities in Figure 14. For a given gas flow rate, the MORS system gives higher RMS liquid velocities than the SOS for the entire reactor region and the draft tube. The difference is more pronounced in the draft tube region. This is again attributed to the lower values of N_{Mal} obtained with the MORS system for a given gas flow rate.

Table II. Percentage of poorly mixed zone in bioreactor for the superficial gas velocities conditions studied for the bioreactor with MORS and SOS.

Superficial gas velocity based on draft tube diameter $\times 10^3$ (m/s)	Percentage dead volume in bioreactor	
	MORS (%)	SOS (%)
1.47	11.52	24.91
4.41	6.46	13.27
7.35	3.48	11.37

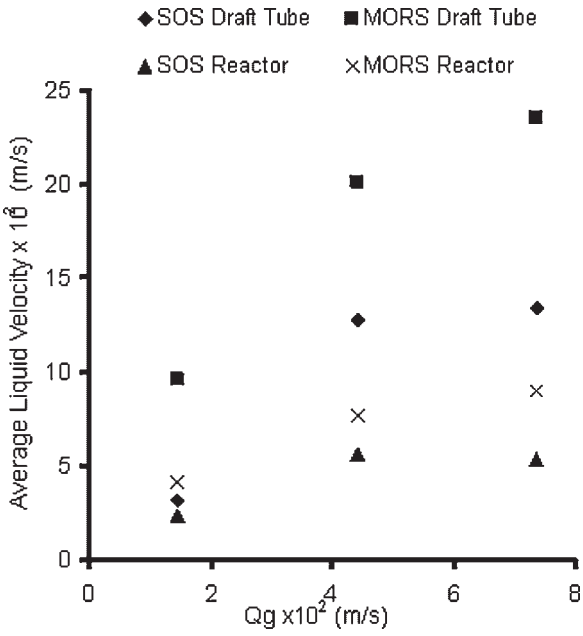

Figure 14. Plot of superficial gas velocity is the draft tube versus time averaged average RMS liquid velocity in the draft tube for the MORS and SOS systems.

DOI 10.1002/bit

Conclusions

The viability of anaerobic bioreactors used for a source of energy generation from organic waste is strongly dependent on their energy economy. The net process energy consumed for proper operation should not exceed the energy available from the biogas (methane) generated. For optimal performance, mixing should be as efficient as possible. CARPT and CT were successfully implemented on a surrogate system to measure gas holdup distribution and liquid velocity and poorly mixed zones in a gas recirculated anaerobic bioreactor.

For a given power input, fixed by the gas flow rate (based on Eq. 1), the MORS was found to gives better gas phase distribution and higher mean gas holdup in the draft tube when compared to SOS. All pores in the MORS do not open, conducting this study at gas flow rates that ensure all the MORS pores are open would have a power input rage that would exceed the recommended range for anaerobic systems (US EPA, 1979). Lower values of N_{Mal} confirm a better performance of the MORS in terms of gas holdup distribution characteristics.

The CARPT results determined that there are poorly mixed zones in the downcomer region of the reactor. Higher liquid velocity values were observed in the draft tube region for the bioreactor with MORS for a fixed gas flow rate. The poorly mixed zones are drastically reduced in the reactor when a MORS system is used as the lower values of gas holdup N_{Mal} in the MORS ensures better liquid circulation. The same trend was observed with the RMS liquid velocity in the entire reactor. Hence the MORS system is considerably more efficient for mixing the reactor than the SOS system. The reduction in the poorly mixed zones would make a larger impact when the bioreactors based on the configurations discussed here are scaled up for pilot plant operations.

Recirculation of the liquid is facilitated by the density gradient between the material in the draft tube and periphery area of the draft tube. This difference triggers the buoyancy forces that enable the liquid to circulate. High gas holdup and better distribution are therefore desirable in the draft tube region to create an effective density gradient for better mixing in the reactor by reducing the fraction of the poorly mixed zones. This objective could be easily achieved with an increase in the superficial gas velocity. However, the energy constraints in such systems give limited flexibility in manipulating the superficial gas velocity as an operation parameter. Hence this necessitates a careful consideration of the sparger design for introducing gas into the system. The impact of the increased and uniform gas holdup distribution in the draft tube, and the reduction in the poorly mixed zones in the bioreactor on the production of methane from bovine waste could be the subject of a performance study. This article confirms that for a given power input, efficiency in mixing can be obtained by appropriate sparger design.

Nomenclature

D_p	diameter of composite radioactive particle (m)
G_r	specific biogas recirculation rate (m^3/dm^3)
g	acceleration due to gravity (m/s)
n_{draft}	number of pixels in the draft tube region
P	power (W/m^3)
P_1	pressure at the injection point (N/m^2) (P_2 + static head of slurry)
P_2	head space pressure (101,416.83 N/m^2)
U_t	terminal settling velocity (m/s)
V	volume of slurry in the system (m^3)
$\langle x \rangle$	notation for image space (pixel index)
ε_g	holdup fraction of gas (dimension less)
ε_L	holdup fraction of liquid (dimension less)
$\overline{\varepsilon}_g$	average gas holdup distribution
ε_g^o	holdup fraction of gas in reactor filled with gas alone (dimension less)
ε_l^o	holdup fraction of gas in reactor filled with slurry alone (dimension less)
λ	1.03
μ_W	viscosity of water in Equation (2) (kg/m-s)
μ_L	ideal attenuation of slurry (m^{-1})
μ_g	ideal attenuation of gas (m^{-1})
$\mu_{EM,g}$	attenuation computed by EM-algorithm for gas (m^{-1})
$\mu_{EM,L}$	attenuation computed by EM-algorithm for slurry (m^{-1})
$\mu_{EM,l-g}$	attenuation computed by EM-algorithm for gas-slurry system (m^{-1})
ρ_p	density of composite radioactive particle (kg/m^3)
ρ_W	density of water (kg/m^3)

The authors would like to acknowledge the United States Department of Energy for sponsoring the research project (Identification number: DE-FC-36-01GO11054).

References

Borole AP, Klasson TK, Ridenour W, Justin H, Karim K, Al-Dahhan MH. 2006. Methane production in a 100-L upflow bioreactor by anaerobic digestion of farm waste. Appl Biochem Biotechnol 131(1–3):887–889.

Casey TJ. 1986. Requirements and methods for mixing in anaerobic digesters. In: Kouzeli-Katsiri A, Bruce AM, Newman PE, editors. Anaerobic digestion of sewage sludge and organic agricultural wastes. Amsterdam: Elsevier Applied Science. p 90–103.

Chisti Y. 1998. Pneumatically agitated bioreactors in industrial and environmental bioprocessing: Hydrodynamics, hydraulics and transport phenomena. Appl Mech Rev Vol 51:33–112.

Degaleesan S. 1997. Fluid dynamics measurement and modeling of liquid mixing in bubble columns. D.Sc. Thesis, Washington University, St. Louis.

Devanathan N. 1991. Investigation of liquid hydrodynamics in bubble column via a computer automated radioactive particle tracking (CARPT). D.Sc. Thesis, Washington University, St. Louis.

George DL, Shollenberger KA, Torczynski JR, O'Hern TJ, Ceccio SL. 2001. Three phase material distribution measurements in a vertical flow using gamma-densitometry tomography and electrical-impedance tomography. Int J Multiphase Flow 27:1903–1930.

Gosh S. 1997. Anaerobic digestion for renewable energy and environmental restoration. In: Proceedings of the Eight International Conference on Anaerobic Digestion. Ministry of Education Japan, Sendai International Center, Sendai, Japan.

Jiang Y. 2000. Flow distribution and it's impact on performance of packed bed reactors. D.Sc. Thesis, Washington University, St. Louis, MO.
Karim K, Thoma GJ. 2007. Gas-Lift digester configuration effects on mixing effectiveness. Water Res (in press).
Karim K, Varma R, Vesvikar V, Al-Dahhan MH. 2004. Flow pattern visualization of a simulated digester. Water Res 38:3659–3670.
Karim K, Hoffmann R, Klasson TK, Al-Dahhan MH. 2005. Anaerobic digestion of animal waste: Effect of mode of mixing. Water Res 39(15): 3597–3606.
Kojima H, Saawai J, Uchina H, Ichige T. 1999. Liquid circulation and Critical gas velocity in slurry bubble column with short size draft tube. Chem Eng Sci 54:5181–5187.
Kumar SB. 1994. Computer tomography measurements of void fraction and modeling of the flow in bubble columns. Ph.D. Thesis, Florida Atlantic University, Boca Raton.
Lange K, Carson R. 1984. EM reconstruction algorithm for emission and transmission tomography. J Comput Assist Tomogr 8(2):306–316.
Lee DJ, Chen GW, Liao YC, Hsieh CC. 1996. On the free-settling test for estimating activated sludge floc density. Water Res 30(3):541–550.
Li X-y, Yuan Y. 2002. Settling velocities and permeabilities of microbial aggregates. Water Res 36(12):3110–3120.
Luo H-P. 2005. Analyzing and modeling of airlift photobioreactors for microalgal and cyanobacteria cultures D.Sc. Thesis, Washington University, St. Louis, MO.
Lusk P. 1998. Methane Recovery from animal manures: A current opportunities casebook. 3rd edition, NREL/SR-580-25145. National Renewable Energy Laboratory, Golden, CO. Work performed by Resource Development Associates, Washington, DC.
Marcandelli C, Lamine AS, Bernard JR, Wild G. 2000. Liquid Distribution in Trickle-bed Reactor. Oil Gas Sci Technol Rev IFP 55(4):407–415.
Ong B. 2003. Experimental investigation of the bubble column hydrodynamics: Effect of elevated pressure and superficial gas velocity. D.Sc. Thesis, Washington University, St. Louis, MO.
Pironti FF, Medina VR, Calvo R, Seaza AE. 1995. Effect of draft tune position on the hydrodynamics of a draft tube slurry bubble column. Chem Eng J 60(1–3):155–160.
Rados N. 2003. Slurry bubble column hydrodynamics. D.Sc. Thesis, Washington University, St. Louis, MO.
Roy S. 2000. Quantification of two-phase flow in liquid-solid risers. D.Sc. Thesis, Washington University St. Louis.
Roy S. 2006. Phase distribution and performance studies of gas-liquid monolith reactors. D.Sc. Thesis, Washington University, St. Louis, MO.
Roy S, Kemoun A, Al-Dahhan MH, Dudukovic' MP, Skourlis TB, Dautzenberg FM. 2004. Countercurrent flow distribution in structured packing via computed tomography. Chem Eng Process 44:59–69.
Sheffield J. 2002. Financial approaches to animal manure management; Joint Institute for Energy and Environment. 314 UT Conference Center Building Knoxville, TN 37996-4138. Report Number: JIEE 2002-04.
Speece RE. 1996. Anaerobic biotechnology for industrial waste waters. Nashville, TN: Vanderbilt University, Arachae Press.
Stroot S, McMahon KD, Mackie RR, Raskin L. 2001. Anaerobic co-digestion of municipal solid waste and biosolids under various mixing conditions-I. Digester performance. Water Res 35 7. 1804–1816.
US EPA. 1979. Process Design Manual for Sludge Treatment and Disposal. EPA 625/1-79-011 Cincinnati, OH.
Vesvikar MS, Al-Dahhan MH. 2005. Flow pattern visualization in a mimic anaerobic digester using CFD. Biotechnol Bioeng 89(6):719–732.
Whitmore TN, Lloyd D, Jones G, Willams TN. 1987. Hydrogen-dependant control of continuous anaerobic digestion process. Appl Microbiol Biotechnol 26:383–388.

DOI 10.1002/bit